

A Constrained, Weighted- ℓ_1 Minimization Approach for Joint Discovery of Heterogeneous Neural Connectivity Graphs

Chandan Singh

University of California, Berkeley

Beilun Wang

University of Virginia

YanJun Qi

University of Virginia

Abstract

Determining functional brain connectivity is crucial to understanding the brain and neural differences underlying disorders such as autism. Recent studies have used Gaussian graphical models to learn brain connectivity via statistical dependencies across brain regions from neuroimaging. However, previous studies often fail to properly incorporate priors tailored to neuroscience, such as preferring shorter connections. To remedy this problem, the paper here introduces a novel, weighted- ℓ_1 , multi-task graphical model (W-SIMULE). This model elegantly incorporates a flexible prior, along with a parallelizable formulation. Additionally, W-SIMULE extends the often-used Gaussian assumption, leading to considerable performance increases. Here, applications to fMRI data show that W-SIMULE succeeds in determining functional connectivity in terms of (1) log-likelihood, (2) finding edges that differentiate groups, and (3) classifying different groups based on their connectivity, achieving 58.6% accuracy on the ABIDE dataset. Having established W-SIMULE's effectiveness, it links four key areas to autism, all of which are consistent with the literature. Due to its elegant domain adaptivity, W-SIMULE can be readily applied to various data types to effectively estimate connectivity.

1 Introduction

Recently, there has been great interest in mapping the interactions between brain regions, a field known as functional connectomics (Smith et al. 2013b). The resulting maps, or connectomes, are fundamental to the study of neuroscience, as having a map of the brain allows for understanding neural pathways and systems (Seung 2011). Furthermore, these connectomes have immediate applications to pathologists trying to understand the neural characteristics underlying clinical disorders (Uddin et al. 2013).

Here, we focus on the important problem of estimating brain connectivity for more than one group (*i.e.* a disease group and a control group). Generally, studies use the simple pairwise correlations (*i.e.* the Pearson correlation coefficient) between the activity of different areas as markers of a connection (Rogers et al. 2007). However, from a neuroscience perspective, this fails to extract the conditional correlations present in the brain and results in spurious connections.

Mathematically, determining functional connectivity amounts to first calculating a covariance matrix (Σ) from the data and then estimating the connectivity graph with the precision matrix ($\Omega = \Sigma^{-1}$). Zeros in Ω correspond to conditionally independent nodes, while non-zero values represent conditional edges (Lauritzen 1996). Recently, Gaussian graphical models (GGMs) have proven to be well-suited to estimating Ω (Koller et al. 2007).

This study's main contribution is the novel formulation of W-SIMULE, which arises naturally from brain-imaging data. W-SIMULE is a weighted- ℓ_1 , multi-task graphical model which robustly estimates Ω for each group. The main advantages of this method are:

- **Effectiveness:** it yields quantifiably accurate connectivity in terms of log-likelihood and classification accuracy
- **Domain adaptivity:** it elegantly enforces a prior based on the problem at hand and can overcome the often-incorrect Gaussian assumption by using nonparanormality
- **Interpretability:** it calculates a connectome for each group which can be tuned to the desired sparsity level and is particularly effective at low sparsity levels
- **Efficiency:** the formulation is column-wise parallelizable and quickly solvable

This study examines a large, resting-state fMRI dataset which serves to compare and validate several recent multi-task learning models. W-SIMULE outperforms other graphical models on this dataset in terms of (1) maximizing the log-likelihood of the connectome, (2) finding edges that differentiate groups, and (3) classifying subjects into their group (autism vs. control). Finally, W-SIMULE is used to analyze the neural basis of autism.

The organization of the paper is as follows: Sec. 2 reviews related work, Sec. 3 develops the model, Sec. 4 shows experiments demonstrating the effectiveness of W-SIMULE, and Sec. 5 explains the conclusions.

2 Background and Related Work

A variety of related work exists. We divide it into four categories: (1) weighted- ℓ_1 models, (2) brain connectivity priors, (3) multi-task brain studies, and (4) multi-task baselines. None of the existing work meets all the specifications of W-SIMULE. Notably, W-SIMULE outperforms all previous

approaches in terms of (1) effectiveness, (2) domain adaptivity, (3) interpretability, and (4) efficiency. Table 1 summarizes the related work. For an overview of ABIDE classification studies, see Appendix Table A1.

Table 1: Summary of related work.

Method	Conditional Independence	Multi-task	Column-wise Parallelizable	Imposes Prior
W-SIMULE	✓	✓	✓	✓
CLIME	✓	✓	×	×
GLASSO	✓	✓	×	×
SIMULE	✓	✓	✓	×
JGL	✓	✓	×	×
SIMONE	✓	✓	×	×
DPM	✓	✓	×	×
Spatial Regularization	×	×	×	✓
Weighted- ℓ_1 GGMs	✓	×	×	✓
sGGGM	✓	✓	×	×
MNS	✓	✓	×	×

Weighted- ℓ_1 Models. ℓ_1 norms effectively induce sparsity in graphical models (Friedman, Hastie, and Tibshirani 2008). Importantly, by weighting the ℓ_1 norm with a prior, the norm can induce sparsity while simultaneously penalizing the selection of certain edges¹. Some recent studies use a weighted- ℓ_1 norm to enforce a prior on a Gaussian graphical model. For example, one model uses reweighted- ℓ_1 norms to maintain sparsity while reducing penalties on nodes with high degree, thus encouraging the appearance of “hub” nodes with a large number of connections (Liu and Ihler 2011). Here, spatial penalization does not necessarily give rise to hub nodes, but rather disincentivizes all nodes from making long connections. Another study uses weighted- ℓ_1 optimization to improve neighborhood selection for gene network estimation (Shimamura et al. 2007). However, no previous weighted- ℓ_1 study extends to multi-task learning or brain connectivity.

Brain Connectivity Priors. W-SIMULE requires choosing a prior to enforce. For fMRI data, spatial distance is a strong candidate, as spatially distant regions are less likely to be connected in the brain (Watts and Strogatz 1998; Vértes et al. 2012). Previous studies have utilized spatial regularization, but use it for smoothing rather than feature selection (Ng and Abugharbieh 2011; Grosenick et al. 2011). Notably, one recent study uses weighted- ℓ_2 regularization to generate ROIs for brain connectivity (Baldassano et al. 2012). Another recent study uses a weighted prior to enhance a neighborhood selection algorithm (Bu and Lederer 2017). There has been some work that aims to derive a population prior to enforce the same pattern of sparsity across

¹This differs from the reweighted- ℓ_1 minimization commonly used in compressed sensing, which typically equips a general linear model to robustly impose sparsity with very few samples (Candes, Wakin, and Boyd 2008).

subjects (Varoquaux et al. 2010), but this differs from the problem here which aims to generate one connectivity graph per group. As an alternative, under the small-world hypothesis, one study aims to decompose whole-brain connectivity into decomposable smaller graphs (Varoquaux et al. 2012).

Multi-task brain studies. Two recent studies apply multi-task learning to brain connectivity determination. MNS (Monti, Anagnostopoulos, and Montana 2015) learns population and subject-specific connectivity in brain networks, but can not effectively discern between two large classes, as is done here. Another recent model, sGGGM (Ng et al. 2013), applies sparsity in a multi-task setting to functional connectivity determination.

Multi-task baselines. W-SIMULE is compared to the two most-cited graphical models for multi-task learning: JGL (Danaher, Wang, and Witten 2014) and SIMONE (Chiquet, Grandvalet, and Ambroise 2011), and two more recent models with formulations closer to the one here: CLIME (Cai, Liu, and Luo 2011) and SIMULE (Wang, Singh, and Qi 2016). Additionally, all models are compared against the extremely popular graphical lasso (GLASSO) (Friedman, Hastie, and Tibshirani 2008). Since previous weighted- ℓ_1 GGMs are not multi-task, comparisons to these models are made by lowering the parameter ϵ to eliminate W-SIMULE’s multi-task component.

3 W-SIMULE: A Weighted- ℓ_1 , Multi-task GGM Model

The main idea behind W-SIMULE is exploiting a prior to jointly estimate connectivity for multiple groups. Figure 1 illustrates this intuition.

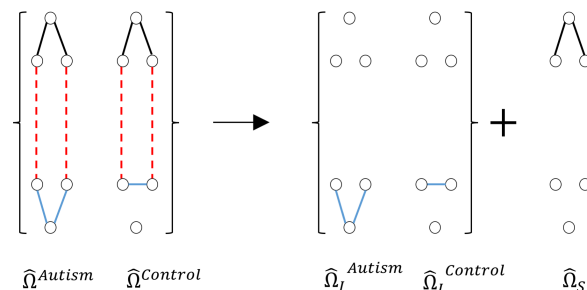


Figure 1: Toy example depicting W-SIMULE. Left shows potential edges present in the data and right shows learned edges. Long edges (red) are spatially penalized and discarded, edges that differ between groups (blue) are learned individually, and edges shared between groups (black) are learned in $\hat{\Omega}_S$.

Algorithm. The problem of determining functional brain connectivity concerns using the covariance matrix (Σ) to calculate the precision matrix ($\Omega = \Sigma^{-1}$), which represents

conditional correlations between brain areas. To do this, W-SIMULE takes advantage of four properties of brain-imaging data (covered in the next four subsections): (a) sparsity, (b) multi-task learning, (c) a prior, and (d) a nonparanormal assumption. In the following work, K is the number of groups, $\|\cdot\|_1$ is the ℓ_1 norm, $\|\cdot\|_\infty$ is the ℓ_∞ norm, W is a prior matrix of positive weights, Σ is the covariance matrix, Ω is the precision matrix, and the dot product (\cdot) between two matrices is their elementwise dot product.

(a) Sparsity. Imposing sparsity is important for interpreting brain connectivity analysis because graphs with too many connections yield very little information. In graphical models, sparsity is generally controlled with an ℓ_1 norm. A simple example of this is the CLIME estimator (Cai, Liu, and Luo 2011), which estimates the precision matrix via constrained- ℓ_1 minimization:

$$\begin{aligned} \widehat{\Omega} &= \underset{\Omega}{\operatorname{argmin}} \|\Omega\|_1 \\ \text{subject to: } & \|\Sigma\Omega - I\|_\infty \leq \lambda \end{aligned} \quad (1)$$

where λ is a hyperparameter controlling the sparsity of Ω .

(b) Multi-task learning. Multi-task learning allows the model to simultaneously estimate more than one group. For example, simply summing CLIME estimators from Eq. (1) over tasks yields a multi-task formulation:

$$\begin{aligned} \widehat{\Omega}^{(1)}, \dots, \widehat{\Omega}^{(K)} &= \underset{\Omega^{(i)}}{\operatorname{argmin}} \sum_i \|\Omega^{(i)}\|_1 \\ \text{subject to: } & \|\Sigma^{(i)}\Omega^{(i)} - I\|_\infty \leq \lambda, i = 1, \dots, K. \end{aligned} \quad (2)$$

where $\Omega^{(i)}$ is the precision matrix for a group i .

It is simple to see that multi-task learning improves performance over single-task models (Evgeniou and Pontil 2004), especially when there are few samples. However, one must choose between two multi-task modeling strategies. The first only models the differences between groups. We ignore this strategy since it does not generate full connectomes for each group, as is desired in many neural applications which require understanding whole-brain connectivity patterns. Instead, we share parameters between different groups. Mathematically, we model $\Omega^{(i)}$ as two parts:

$$\Omega^{(i)} = \Omega_I^{(i)} + \Omega_S \quad (3)$$

where $\Omega_I^{(i)}$ is the individual precision matrix for group i and Ω_S is the shared precision matrix between groups. This yields the following formulation:

$$\begin{aligned} \widehat{\Omega}_I^{(1)}, \dots, \widehat{\Omega}_I^{(K)}, \widehat{\Omega}_S &= \sum_i \underset{\Omega_I^{(i)}, \Omega_S}{\operatorname{argmin}} \|\Omega_I^{(i)}\|_1 + \epsilon K \|\Omega_S\|_1 \\ \text{subject to: } & \|\Sigma^{(i)}(\Omega_I^{(i)} + \Omega_S) - I\|_\infty \leq \lambda, i = 1, \dots, K. \end{aligned} \quad (4)$$

(c) Weighted prior. Over time, neuroscientists have gathered considerable knowledge regarding the spatial and anatomical priors underlying brain connectivity (*i.e.* short edges and certain anatomical regions are more likely to be connected (Watts and Strogatz 1998)). Previous studies (see Sec. 2) enforce these priors via a matrix of weights, W , corresponding to edges. Existing brain connectivity studies enforce a spatial prior using a weighted- ℓ_2 norm (Ng and Abugarbieh 2011; Groseknick et al. 2011; Baldassano et al. 2012), resulting in the following penalization term: $\|W \cdot \Omega\|_2$. This weighted- ℓ_2 norm effectively imposes spatial smoothness. Other studies, unrelated to brain connectivity, use a weighted- ℓ_1 norm to enforce a prior in a graphical model: $\|W \cdot \Omega\|_1$. Here, we opt for the ℓ_1 norm, as it effectively combines the prior with sparsity (Shimamura et al. 2007).

(d) Nonparanormal Extension. In addition to Gaussian data, W-SIMULE supports nonparanormal Gaussian data (we refer to the nonparanormal version as W-SIMULE and the Gaussian version as W-SIMULEG). This is implemented by using the Kendall correlation matrix (Σ_N) of the data matrices rather than the sample covariance matrix (Σ). This allows W-SIMULE to fit many datasets that violate the often-used Gaussian assumption by fitting a nonparanormal distribution (Liu, Lafferty, and Wasserman 2009).

W-SIMULE: Putting it all together. Combining the elements of sparsity, multi-task learning, a weighted prior, and a nonparanormal assumption yields the novel formulation of W-SIMULE:

$$\begin{aligned} \widehat{\Omega}_I^{(1)}, \dots, \widehat{\Omega}_I^{(K)}, \widehat{\Omega}_S &= \sum_i \underset{\Omega_I^{(i)}, \Omega_S}{\operatorname{argmin}} \|W \cdot \Omega_I^{(i)}\|_1 + \epsilon K \|W \cdot \Omega_S\|_1 \\ \text{Subject to: } & \|\Sigma_N^{(i)}(\Omega_I^{(i)} + \Omega_S) - I\|_\infty \leq \lambda, i = 1, \dots, K. \end{aligned} \quad (5)$$

W-SIMULE has three hyperparameters (W , λ , and ϵ) that make it incredibly flexible. Using a different W can enforce a different prior or change how strictly a prior is enforced. Next, changing the hyperparameter λ controls the total sparsity of the resulting precision matrices. Finally, changing the hyperparameter ϵ allows for controlling how strictly the group penalty is imposed, *i.e.* the relative sparsities between the shared parameters and the individual parameters.

Optimization. Eq. (5) can be solved in parallel for each column j :

$$\underset{\beta^{(i)}, \beta^s}{\operatorname{argmin}} \sum_i \|W_{\cdot j} \cdot \beta^{(i)}\|_1 + \epsilon K \|W_{\cdot j} \cdot \beta^s\|_1 \quad (6)$$

$$\text{Subject to: } \|\Sigma^{(i)}(\beta^{(i)} + \beta^s) - e_j\|_\infty \leq \lambda, i = 1, \dots, K$$

where $W_{\cdot j}$ is the j -th column of W , $\beta^{(i)}$ is the j -th column of $\Omega_I^{(i)}$ of i -th graph (we take out the subscript I in $\beta^{(i)}$ to

simplify notations), and β^s is the corresponding column in the shared part Ω_S . Simplifying Eq. (6) yields

$$\operatorname{argmin}_{\theta} \|W_{:,j} \cdot \theta\|_1 \quad (7)$$

Subject to: $\|\mathbf{A}^{(i)}\theta - b\|_{\infty} \leq c, i = 1, \dots, K$

Where $\mathbf{A}^{(i)} = [0, \dots, 0, \Sigma^{(i)}, 0, \dots, 0, \frac{1}{\epsilon K} \Sigma^{(i)}]$,

$\theta = [\beta^{(1)T}, \dots, \beta^{(K)T}, \epsilon K (\beta^s)^T]^T$,

$b = \mathbf{e}_j, c = \lambda$

Algorithm 1 A Weighted- ℓ_1 , Multi-task Graphical Model (W-SIMULE)

Input: Data matrices $\mathbf{X}^{(1)}, \dots, \mathbf{X}^{(K)}$, regularization hyperparameter λ , hyperparameter ϵ , and linear programming solver $\mathbf{LP}(\cdot)$, which solves Eq. (7)

Output: Shared graph Ω_S and individual graphs $\Omega_I^{(1)}, \dots, \Omega_I^{(K)}$

```

1: for  $i = 1$  to  $K$  do
2:   Initialize  $\Sigma^{(i)}$  as the sample cov. matrix of  $\mathbf{X}^{(i)}$ 
3:   Initialize  $\Omega_I^{(i)} = \mathbf{0}_{p \times p}$ 
4:   Initialize  $\mathbf{A}^{(i)} = [0, \dots, 0, \Sigma^{(i)}, 0, \dots, 0, \frac{1}{\epsilon K} \Sigma^{(i)}]$ 
5: end for
6: Initialize  $\Omega_S = \mathbf{0}_{p \times p}$ 
7: for  $j = 1$  to  $p$  do
8:    $\theta = \mathbf{LP}(\mathbf{A}^{(i)}, b = \mathbf{e}_j, c = \lambda)$  where  $i = 1, \dots, K$ 
9:   for  $i = 1$  to  $K$  do
10:     $\Omega_{I,j}^{(i)} = \theta_{((i-1)p+1):ip}$ 
11:   end for
12:    $\Omega_{S,j} = \theta_{(Kp+1):(K+1)p}$ 
13: end for

```

To solve Eq. (7), we follow the simplex method (Pang, Liu, and Vanderbei 2014), which is empirically faster than the primal dual interior method (Cormen 2009). The final formulation becomes

$$\operatorname{argmin}_{\theta^+, \theta^-} W_{:,j} \cdot \theta^+ + W_{:,j} \cdot \theta^-$$

Subject to :

$$\begin{pmatrix} \mathbf{A}^{(i)} & -\mathbf{A}^{(i)} \\ -\mathbf{A}^{(i)} & \mathbf{A}^{(i)} \end{pmatrix} \begin{pmatrix} \theta^+ \\ \theta^- \end{pmatrix} \leq \begin{pmatrix} c + b \\ c - b \end{pmatrix} \quad (8)$$

$$\begin{pmatrix} \theta^+ \\ \theta^- \end{pmatrix} \geq 0$$

where θ^+ and θ^- refer to the positive and negative parts of θ , respectively.

W-SIMULE is summarized in Algorithm 1. Following CLIME, we then apply the same symmetric operators on $\{\Omega^{(i)} = \Omega_S + \Omega_I^{(i)}\}$ obtained from Algorithm 1.

Each column of W-SIMULE can be solved in parallel. Algorithm 1 can be revised into a parallel version by modifying the “for loop” of step 7 in Algorithm 1 into a “parallel for loop” over columns. The model’s convergence follows from the proven convergence of SIMULE (Wang, Singh, and Qi 2016) and the fact that the positive weights in W yield a convex norm.

4 Experiments

This section reports experiments showing the effectiveness of W-SIMULE. It begins with the experimental setup in subsection 4.1, then details experiments showing effectiveness in subsection 4.2, and finally gives neuroscientific validation in subsection 4.3.

4.1 Experimental Setup

Data. The data examined here comes from the Autism Brain Imaging Data Exchange (ABIDE) (Di Martino et al. 2014), a publicly available resting-state fMRI dataset. The ABIDE data was released with the goal of understanding human brain connectivity and how it reflects neural disorders (Van Essen et al. 2013). The data was retrieved from the Preprocessed Connectomes Project (Craddock 2014), where preprocessing was performed using the Configurable Pipeline for the Analysis of Connectomes (CPAC) (Craddock et al. 2013) without global signal correction or band-pass filtering. After preprocessing with this pipeline, 871 individuals remain (468 diagnosed with autism). Signals for the 160 regions of interest (ROIs) in the often-used Dosenbach Atlas (Dosenbach et al. 2010) are examined.

Priors. To select the prior W , two separate spatial priors were derived from the Dosenbach atlas. The first, referred to as *anatomicalⁱ*, gives each ROI one of 40 well-known, anatomic labels (e.g. “basal ganglia”, “thalamus”). Weights take the low value i if two ROIs have the same label, and the high value $10 - i$ otherwise. The second prior, referred to as *distⁱ*, sets the weight of each edge to its spatial length, in MNI space², raised to the power i .

Cross-validation. Classification is performed using 3-fold cross validation, an important step in fMRI analysis (Poldrack et al. 2008), but often neglected in the literature until recently (Varoquaux et al. 2010). The subjects are randomly partitioned into 3 equal sets: a training set, a validate set, and a test set. Each model produces $\hat{\Omega}^{\text{control}}$ and $\hat{\Omega}^{\text{autism}}$ using the training set. Then, these graphs are fed as inputs to linear discriminant analysis (LDA), which is tuned via cross-validation on the validate set. Finally, accuracy is calculated by running LDA on the test set. Importantly, this process the ability of a method to learn the connectome’s structure. The full process is performed and averaged over three folds for each model covered in Sec. 2 which produces a connectome. Notably, some of the methods (e.g. DPM) cannot be compared against, as they do not provide the precision matrices necessary for LDA. Other methods, (e.g. MNS) fail to converge when run on the dataset, as they can not handle a large number of subjects in each group.

4.2 Empirical Effectiveness

Log-likelihood. The most often-used metric for comparing graphs generated by graphical models is the log-likelihood. Here, connectomes are generated for various

²MNI space is a coordinate system used to refer to analagous points on different brains.

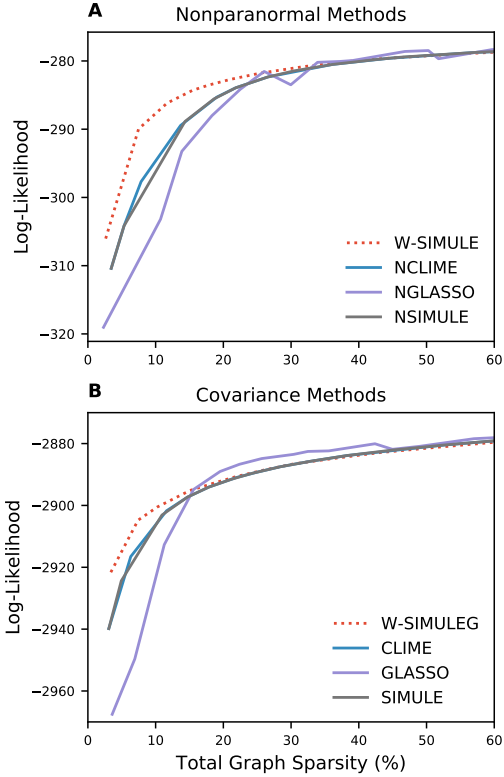


Figure 2: Model performance measured by log-likelihood. **A** and **B** show the log-likelihood versus number edges included in the model. Note that **A** and **B** are not directly comparable, as **A** uses the nonparanormal versions of the models in **B**. Both JGL and SIMONE are not shown as they yield log-likelihood values too low to be plotted on these graphs.

sparsity levels and their resulting log-likelihoods are plotted in Fig 2.³ Unsurprisingly, as the number of total edges included in the graphs increases, the log-likelihood of the model increases. W-SIMULE ($\epsilon = 1$, $W = dist^2$), shown as the dotted red line, outperforms all of the relevant baselines, especially at low sparsities, which are most biophysically plausible. Intuitively, this suggests that W-SIMULE can find the fewest edges which explain the most observed data. This is a very useful property to neuroscientists who seek interpretable connectomes. Without the nonparanormal assumption, W-SIMULEG only outperforms other baselines at low sparsities.

Classification Accuracy. Table 2 displays the maximum accuracy achieved for each baseline, after sweeping over hyperparameters. W-SIMULE ($\epsilon = 1$, $W = anatomical^2$, $\lambda = 0.04$) yields a classification accuracy of 58.62% between the autism and control groups, outperform-

³All models were also run with intertwined covariances (covariances generated in a multi-task setting), but the results did not improve and are omitted.

ing other state-of-the-art graphical models.

Table 2: Classification accuracy obtained on the ABIDE dataset using various methods. W-SIMULE has the highest accuracy of all the values in the table.

Method	Accuracy (%)
W-SIMULE	58.62%
CLIME	46.55%
GLASSO	53.71%
SIMULE	57.96%
JGL (fused)	56.90%
SIMONE	53.71%

Parameter variation. The results are fairly robust to variations of the prior (see Table 3A). The effect of changing the prior seems to have a fairly small effect on the log-likelihood of the model. This is likely because all examined priors penalize picking physically long edges, which agrees with observations from neuroscience. The *dist* prior effectively encourages the selection of short edges (see Appendix Fig A1), and the *anatomical* prior also has substantial spatial localization.

Table 3B shows that the effect of changing ϵ (the strength of the multi-task component). The log-likelihood is robust to variations in ϵ over a certain range, but can change significantly if ϵ varies drastically. The same goes for the test accuracy. Generally, as ϵ gets larger, thus increasing the importance of the shared parameters between groups, the log-likelihood increases. This emphasizes the importance of the multi-task term of W-SIMULE. Since the total number of subjects is limited, strengthening the multi-task component effectively doubles the sample size (including both classes) and allows for better picking edges.

Table 3: Variations of the prior and multi-task component yield fairly stable results.

A: Varying Prior ($\epsilon = 1$)				
Prior	Log-Likelihood	Test Accuracy	Log-Likelihood	Test Accuracy
	Sparsity=8%	Sparsity=8%	Sparsity=16%	Sparsity=16%
<i>No prior</i>	-295.98	0.56	-286.17	0.55
<i>dist</i>	-290.71	0.54	-284.63	0.56
<i>dist</i> ²	-289.55	0.54	-283.89	0.54
<i>anatomical</i> ¹	-290.84	0.55	-283.69	0.56
<i>anatomical</i> ²	-292.14	0.58	-284.72	0.55

B: Varying ϵ (Prior = <i>anatomical</i> ²)				
ϵ	Log-Likelihood	Test Accuracy	Log-Likelihood	Test Accuracy
	Sparsity=8%	Sparsity=8%	Sparsity=16%	Sparsity=16%
1.6	-292.14	0.58	-284.72	0.54
1.2	-292.13	0.58	-284.71	0.54
1.0	-292.14	0.58	-284.72	0.55
0.6	-301.72	0.55	-294.91	0.54

4.3 Neuroscientific validation

Connectome. W-SIMULE yields different connectomes depending on its hyperparameters. Here, Fig 3 shows the connectome which yielded the maximum accuracy in Table 2, generated using W-SIMULE ($\epsilon = 1$, $W = anatomical^2$, $\lambda = 0.04$). In order to be interpretable, only 2.5% of the possible edges were visualized (the same set of possible edges is visualized for both the autism and control groups). Note that many edges are shared between the groups, emphasizing the need for multi-task learning.

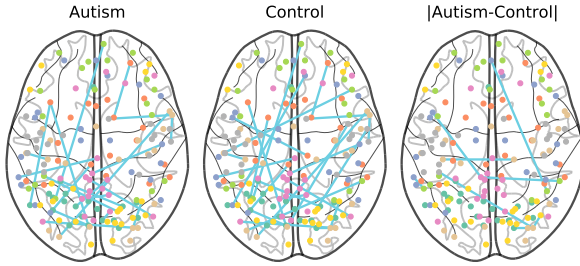


Figure 3: Sparse connectome generated by W-SIMULE using the $anatomical^2$ prior. The autism graph, control graph, and their difference are shown. Many edges are shared between the groups. Visualized with nilearn (Abraham et al. 2014).

Autism-specific areas. To analyze neural differences, we average over several connectomes. Again using $\epsilon = 1$ and $W = anatomical^2$, sweeping over different values of λ yields connectomes at various sparsity levels. At each sparsity level, we calculate the difference between the autism and control group, as seen in Fig. 3. On average, the edges that connect to the following four areas are most affected (in decreasing order): the precuneus, the basal ganglia, the anterior cingulate cortex, and the medial frontal cortex. These results are consistent with the findings of previous brain-imaging studies. For example, some find significant under-connectivity to and from the precuneus in autistic subjects (Cherkassky et al. 2006). Together, the medial frontal cortex and anterior cingulate cortex have been linked to the neural basis of social impairments in autism (Mundy 2003). Finally, the changes in the basal ganglia due to autism reflect changes in gait of autism patients (Rinehart et al. 2006). These results serve as validation for W-SIMULE, but note that the analysis here yields no information about the neural connections within these fairly large areas. In order to find more detailed information within one of these areas, one could run W-SIMULE using an atlas more refined than the Dosenbach atlas, which divides the brain into just 160 ROIs.

5 Conclusions

Here, we develop W-SIMULE, which effectively generates quantifiable, state-of-the-art connectivity. W-SIMULE is highly effective and easily adapts to different domains. Connectomes generated by W-SIMULE selectively highlight

connections that are important for distinguishing between autism and control groups (see Figure 2B, Table 2) and can be used to analyze the connectome (see subsection 4.3). W-SIMULE can help researchers to pinpoint the neural basis of autism or other disorders with large fMRI datasets (Milham et al. 2012; Smith et al. 2013a).

W-SIMULE has great potential for future applications. As brain-imaging datasets become more complex and include more structural data (e.g. MRI) coupled with functional data (e.g. fMRI), W-SIMULE will become increasingly important to neuroscience. This is especially true for studies with small sample sizes, such as task-specific studies, which require strong priors and multi-task learning in order to robustly determine connectivity (Real et al. 2017). As the spatial resolution of fMRI increases, spatial penalization will become more important in constructing accurate ROIs and brain connections (Craddock, Tuncaraza, and Milham 2015; Thirion et al. 2014). Finally, many problems outside of neuroscience can benefit from W-SIMULE; it can utilize diverse priors to find conditional independence between nodes in any multi-task setting. Thus, W-SIMULE can be readily applied to gene-network estimation (Shimamura et al. 2007), computer vision (where physical distance could be used as a prior in images), and many other problems that currently utilize Gaussian graphical models.

Appendix

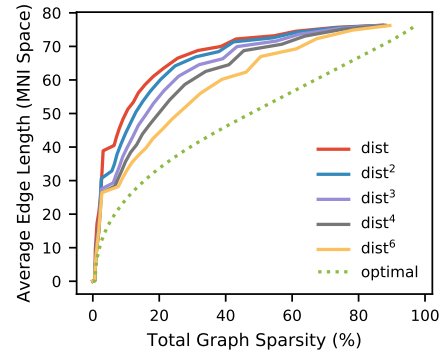


Figure A1: W-SIMULE effectively enforces the prior. As the $dist$ prior is raised to a higher power (thereby increasing the spread of the weights in the matrix W), the prior is more strictly enforced. This results in a lower average edge length at every sparsity level. The dotted “optimal” line shows the lowest possible average edge length as a function of graph sparsity. Here, W-SIMULE uses $\epsilon = 1$ and λ is varied to yield different sparsities.

Table A1: Classification accuracy obtained on ABIDE dataset by various studies. In general, classifiers significantly improve over randomness (50%). These studies are not directly comparable to W-SIMULE. Most take drastically different approaches and do not provide a full, interpretable connectome as W-SIMULE does. Instead, many classify without learning the connectivity structure (e.g. with a neural network). The accuracy score also does not consider sparsity, domain adaptivity, or efficiency. Preprocessing, training, and validation schemes varies between the studies. Smaller subsets of the data are generally able to achieve better performance.

Study	Method	Total Subjects	Autism Subjects	Control Subjects	Accuracy (%)
Ghiassian et al. 2013	MRMR	1111	538	573	63
Nielsen et al. 2013	GLM	964	447	517	60
Haar et al. 2014	LDA/ QDA	906	453	453	~50
W-SIMULE	LDA	871	403	468	58.6
Parisot et al. 2017	Graph CNN	871	403	468	69.5
Abraham et al. 2017	See paper	871	403	468	66.8
Iidaka 2015	PNN	640	328	312	90
Haar et al. 2014	LDA/ QDA	590	295	295	60
Chen et al. 2015	RF	252	126	126	91
Chen et al. 2016	SVM	240	112	128	79
Plitt, Barnes, and Martin 2015	L2LR	178	89	89	71

References

Abraham, A.; Pedregosa, F.; Eickenberg, M.; Gervais, P.; Muller, A.; Kossaiji, J.; Gramfort, A.; Thirion, B.; and Varoquaux, G. 2014. Machine learning for neuroimaging with scikit-learn. *arXiv preprint arXiv:1412.3919*.

Abraham, A.; Milham, M. P.; Di Martino, A.; Craddock, R. C.; Samaras, D.; Thirion, B.; and Varoquaux, G. 2017. Deriving reproducible biomarkers from multi-site resting-state data: An autism-based example. *NeuroImage* 147:736–745.

Baldassano, C.; Iordan, M. C.; Beck, D. M.; and Fei-Fei, L. 2012. Voxel-level functional connectivity using spatial regularization. *Neuroimage* 63(3):1099–1106.

Bu, Y., and Lederer, J. 2017. Integrating additional knowledge into estimation of graphical models. *arXiv preprint arXiv:1704.02739*.

Cai, T.; Liu, W.; and Luo, X. 2011. A constrained l_1 minimization approach to sparse precision matrix estimation. *Journal of the American Statistical Association* 106(494):594–607.

Candes, E. J.; Wakin, M. B.; and Boyd, S. P. 2008. Enhancing sparsity by reweighted l_1 minimization. *Journal of Fourier analysis and applications* 14(5-6):877–905.

Chen, C. P.; Keown, C. L.; Jahedi, A.; Nair, A.; Pflieger, M. E.; Bailey, B. A.; and Müller, R.-A. 2015. Diagnostic classification of intrinsic functional connectivity highlights somatosensory, default mode, and visual regions in autism. *NeuroImage: Clinical* 8:238–245.

Chen, H.; Duan, X.; Liu, F.; Lu, F.; Ma, X.; Zhang, Y.; Uddin, L. Q.; and Chen, H. 2016. Multivariate classification of autism spectrum disorder using frequency-specific resting-state functional connectivity multi-center study. *Progress in Neuro-Psychopharmacology and Biological Psychiatry* 64:1–9.

Cherkassky, V. L.; Kana, R. K.; Keller, T. A.; and Just, M. A. 2006. Functional connectivity in a baseline resting-state network in autism. *Neuroreport* 17(16):1687–1690.

Chiquet, J.; Grandvalet, Y.; and Ambroise, C. 2011. Inferring multiple graphical structures. *Statistics and Computing* 21(4):537–553.

Cormen, T. H. 2009. *Introduction to algorithms*. MIT press.

Craddock, C.; Sikka, S.; Cheung, B.; Khanuja, R.; Ghosh, S.; Yan, C.; Li, Q.; Lurie, D.; Vogelstein, J.; Burns, R.; et al. 2013. Towards automated analysis of connectomes: The configurable pipeline for the analysis of connectomes (c-pac). *Front Neuroinform* 42.

Craddock, R. C.; Tungaraza, R. L.; and Milham, M. P. 2015. Connectomics and new approaches for analyzing human brain functional connectivity. *GigaScience* 4(1):13.

Craddock, C. 2014. Preprocessed connectomes project: open sharing of preprocessed neuroimaging data and derivatives. In *61st Annual Meeting. AACAP*.

Danaher, P.; Wang, P.; and Witten, D. M. 2014. The joint graphical lasso for inverse covariance estimation across multiple classes. *Journal of the Royal Statistical Society: Series B (Statistical Methodology)* 76(2):373–397.

Di Martino, A.; Yan, C.-G.; Li, Q.; Denio, E.; Castellanos, F. X.; Alaerts, K.; Anderson, J. S.; Assaf, M.; Bookheimer, S. Y.; Dapretto, M.; et al. 2014. The autism brain imaging data exchange: towards a large-scale evaluation of the intrinsic brain architecture in autism. *Molecular psychiatry* 19(6):659–667.

Dosenbach, N. U.; Nardos, B.; Cohen, A. L.; Fair, D. A.; Power, J. D.; Church, J. A.; Nelson, S. M.; Wig, G. S.; Vogel, A. C.; Lessov-Schlaggar, C. N.; et al. 2010. Prediction of individual brain maturity using fmri. *Science* 329(5997):1358–1361.

Evgeniou, T., and Pontil, M. 2004. Regularized multi-task learning. In *Proceedings of the tenth ACM SIGKDD international conference on Knowledge discovery and data mining*, 109–117. ACM.

Friedman, J.; Hastie, T.; and Tibshirani, R. 2008. Sparse inverse covariance estimation with the graphical lasso. *Biostatistics* 9(3):432–441.

Ghiassian, S.; Greiner, R.; Jin, P.; and Brown, M. 2013. Learning to classify psychiatric disorders based on fmri images: Autism vs healthy and adhd vs healthy. In *Proceedings of 3rd NIPS Workshop on Machine Learning and Interpretation in NeuroImaging*.

Grosenick, L.; Klingenberg, B.; Knutson, B.; and Taylor, J. 2011. A family of interpretable multivariate models for regression and classification of whole-brain fmri data. *arXiv preprint arXiv:1110.4139*.

Haar, S.; Berman, S.; Behrmann, M.; and Dinstein, I. 2014. Anatomical abnormalities in autism? *Cerebral Cortex* bhu242.

Iidaka, T. 2015. Resting state functional magnetic resonance imaging and neural network classified autism and control. *Cortex* 63:55–67.

Koller, D.; Freedman, N.; Getoor, L.; and Taskar, B. 2007. Graphical models in a nutshell in introduction to statistical relational learning. *Stanford*.

- Lauritzen, S. L. 1996. *Graphical models*, volume 17. Clarendon Press.
- Liu, Q., and Ihler, A. T. 2011. Learning scale free networks by reweighted l1 regularization. In *AISTATS*, 40–48.
- Liu, H.; Lafferty, J.; and Wasserman, L. 2009. The nonparanormal: Semiparametric estimation of high dimensional undirected graphs. *Journal of Machine Learning Research* 10(Oct):2295–2328.
- Milham, M. P.; Fair, D.; Mennes, M.; Mostofsky, S. H.; et al. 2012. The adhd-200 consortium: a model to advance the translational potential of neuroimaging in clinical neuroscience. *Frontiers in systems neuroscience* 6:62.
- Monti, R. P.; Anagnostopoulos, C.; and Montana, G. 2015. Learning population and subject-specific brain connectivity networks via mixed neighborhood selection. *arXiv preprint arXiv:1512.01947*.
- Mundy, P. 2003. Annotation: The neural basis of social impairments in autism: the role of the dorsal medial-frontal cortex and anterior cingulate system. *Journal of Child Psychology and psychiatry* 44(6):793–809.
- Ng, B., and Abugharbieh, R. 2011. Generalized sparse regularization with application to fmri brain decoding. In *Biennial International Conference on Information Processing in Medical Imaging*, 612–623. Springer.
- Ng, B.; Varoquaux, G.; Poline, J. B.; and Thirion, B. 2013. A novel sparse group gaussian graphical model for functional connectivity estimation. In *International Conference on Information Processing in Medical Imaging*, 256–267. Springer.
- Nielsen, J. A.; Zielinski, B. A.; Fletcher, P. T.; Alexander, A. L.; Lange, N.; Bigler, E. D.; Lainhart, J. E.; and Anderson, J. S. 2013. Multisite functional connectivity mri classification of autism: Abide results. *Frontiers in Human Neuroscience* 7.
- Pang, H.; Liu, H.; and Vanderbei, R. J. 2014. The fastclime package for linear programming and large-scale precision matrix estimation in r. *Journal of Machine Learning Research* 15(1):489–493.
- Parisot, S.; Ktena, S. I.; Ferrante, E.; Lee, M.; Moreno, R. G.; Glocker, B.; and Rueckert, D. 2017. Spectral graph convolutions on population graphs for disease prediction. *arXiv preprint arXiv:1703.03020*.
- Plitt, M.; Barnes, K. A.; and Martin, A. 2015. Functional connectivity classification of autism identifies highly predictive brain features but falls short of biomarker standards. *NeuroImage: Clinical* 7:359–366.
- Poldrack, R. A.; Fletcher, P. C.; Henson, R. N.; Worsley, K. J.; Brett, M.; and Nichols, T. E. 2008. Guidelines for reporting an fmri study. *Neuroimage* 40(2):409–414.
- Real, E.; Asari, H.; Gollisch, T.; and Meister, M. 2017. Neural circuit inference from function to structure. *Current Biology*.
- Rinehart, N. J.; Tonge, B. J.; Iasek, R.; McGinley, J.; Brereton, A. V.; Enticott, P. G.; and Bradshaw, J. L. 2006. Gait function in newly diagnosed children with autism: cerebellar and basal ganglia related motor disorder. *Developmental Medicine & Child Neurology* 48(10):819–824.
- Rogers, B. P.; Morgan, V. L.; Newton, A. T.; and Gore, J. C. 2007. Assessing functional connectivity in the human brain by fmri. *Magnetic resonance imaging* 25(10):1347–1357.
- Seung, H. S. 2011. Neuroscience: towards functional connectomics. *Nature* 471(7337):170–172.
- Shimamura, T.; Imoto, S.; Yamaguchi, R.; and Miyano, S. 2007. Weighted lasso in graphical gaussian modeling for large gene network estimation based on microarray data. *Genome Informatics* 19:142–153.
- Smith, S. M.; Beckmann, C. F.; Andersson, J.; Auerbach, E. J.; Bijsterbosch, J.; Douaud, G.; Duff, E.; Feinberg, D. A.; Griffanti, L.; Harms, M. P.; et al. 2013a. Resting-state fmri in the human connectome project. *Neuroimage* 80:144–168.
- Smith, S. M.; Vidaurre, D.; Beckmann, C. F.; Glasser, M. F.; Jenkinson, M.; Miller, K. L.; Nichols, T. E.; Robinson, E. C.; Salimi-Khorshidi, G.; Woolrich, M. W.; et al. 2013b. Functional connectomics from resting-state fmri. *Trends in cognitive sciences* 17(12):666–682.
- Thirion, B.; Varoquaux, G.; Dohmatob, E.; and Poline, J.-B. 2014. Which fmri clustering gives good brain parcellations? *Frontiers in neuroscience* 8:167.
- Uddin, L. Q.; Supekar, K.; Lynch, C. J.; Khouzam, A.; Phillips, J.; Feinstein, C.; Ryali, S.; and Menon, V. 2013. Salience network-based classification and prediction of symptom severity in children with autism. *JAMA psychiatry* 70(8):869–879.
- Van Essen, D. C.; Smith, S. M.; Barch, D. M.; Behrens, T. E.; Yacoub, E.; Ugurbil, K.; Consortium, W.-M. H.; et al. 2013. The wu-minn human connectome project: an overview. *Neuroimage* 80:62–79.
- Varoquaux, G.; Gramfort, A.; Poline, J.-B.; and Thirion, B. 2010. Brain covariance selection: better individual functional connectivity models using population prior. In *Advances in neural information processing systems*, 2334–2342.
- Varoquaux, G.; Gramfort, A.; Poline, J. B.; and Thirion, B. 2012. Markov models for fmri correlation structure: is brain functional connectivity small world, or decomposable into networks? *Journal of physiology-Paris* 106(5):212–221.
- Vértes, P. E.; Alexander-Bloch, A. F.; Gogtay, N.; Giedd, J. N.; Rapoport, J. L.; and Bullmore, E. T. 2012. Simple models of human brain functional networks. *Proceedings of the National Academy of Sciences* 109(15):5868–5873.
- Wang, B.; Singh, R.; and Qi, Y. 2016. A constrained l1 minimization approach for estimating multiple sparse gaussian or nonparanormal graphical models. *arXiv preprint arXiv:1605.03468*.
- Watts, D. J., and Strogatz, S. H. 1998. Collective dynamics of small-worldnetworks. *nature* 393(6684):440–442.